Author's copy. Appeared in Short Paper Proceedings of IEEE Pacific Visualization Symposium (PacificVIS).

Visualization of Fullerene Fragmentation

Kai Sdeo* Bastian Rieck† Filip Sadlo‡

Heidelberg University, Germany

Abstract

In this paper, we present a novel visualization approach for the analysis of fragmentation of molecules, with a particular focus on fullerenes. Our approach consists of different components at different levels of detail. Whereas one component is geometric but invariant to rotations, two other components are based on the topological structure of the molecules and thus additionally invariant to deformations. By combining these three components, which aim at the analysis of simulation ensembles of such molecules, and complementing them with a space-time representation that enables detailed interactive inspection of individual simulations, we obtain a versatile tool for the analysis of the fragmentation of structured, symmetrical molecules such as fullerenes. We exemplify the utility of our approach using a tightly coupled simulation approach for the dynamics of fullerenes.

Index Terms: Computing methodologies—Modeling and simulation—Simulation types and techniques—Scientific visualization; Human-centered computing—Visualization—Visualization application domains—Scientific visualization

1 Introduction

Carbon is an integral part of all known lifeforms. Not only is it a vital component in building cells for living organisms, but it also gives rise to a rich variety of potential chemical bindings with exceptional properties. Often, carbon is studied in the form of fullerenes, a category of carbon-based molecules that have seen many uses, including semiconductors and superconductors. Among the fullerenes, C_{60} (Figure 1a), also known as the buckyball, is of particular interest. Having sixty atoms, it is large enough to result in a complex system of coupled atom–atom interactions, and its symmetrical genus-zero structure makes it an ideal example for studying complex carbon bond systems, both experimentally and theoretically. To study bonds of C_{60} experimentally, techniques such as laser pulse excitation are commonly employed, which ionize the molecule and may tear it apart into molecular fragments. While the final products of such decay processes have already been studied extensively, the dynamics of these processes remain an active research topic.

Since the experimental setups are, however, costly and time-consuming, and typically cannot investigate individual molecules, simulation and visualization aid the investigation of laser–fullerene interactions with a special focus on its fragmentation. In this work, we are particularly interested in comparing different simulations among each other, in order to (i) analyze their average behavior, (ii) study the influence of initial parameters, and (iii) highlight interesting phenomena of a fragmentation process. To this end, we introduce novel visualization techniques, encompassing different levels of detail that range from highly coarse (characteristic curves) to extremely detailed (fragmentation trees).

*e-mail: kai.sdeo@iwr.uni-heidelberg.de
†e-mail: bastian.rieck@iwr.uni-heidelberg.de
‡e-mail: sadlo@uni-heidelberg.de

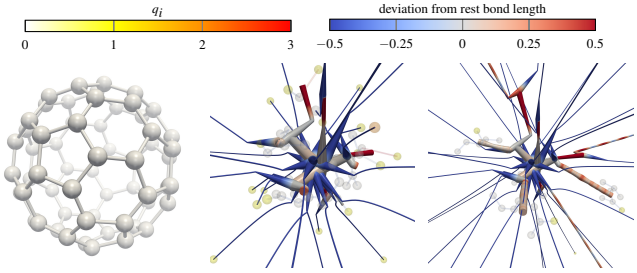

Figure 1: Fragmentation process of a fullerene C_{60} that is positively ionized by 44 elementary charges ($q_{\text{mean}} = 40$, see Section 4). (a) Initial state, not charged, state at (b) $t = 125\,\text{fs}$, and (c) $t = 375\,\text{fs}$ of the fragments. The molecule is represented with the ball-and-stick model together with the fragment tree (colored), our space-time representation of its dynamics. Atoms (balls) are colored by their charge q_i (in elementary charges). The deviation from the bond rest length (in Å) is encoded in bonds (sticks) and in the fragment tree, which is color-coded according to the maximum bond length of the corresponding molecule fragment.

Our simulations are realized in the molecular dynamics framework LAMMPS [11], which is capable of simulating intermolecular forces. Each simulation addresses a single molecule, and follows physical experiments by ionizing individual atoms of the molecule, with Gaussian probability distribution. Ionization happens independently of the position of a given atom, and in turn triggers Coulomb forces that cause charged atoms to repel each other, possibly breaking molecular bonds, and eventually leading to fragmentation.

2 Related Work

Molecular dynamics simulations are a common tool for investigating fullerenes [9, 16]. Previous work on the analysis of the resulting data includes an approach based on relative distances, in the context of a low-velocity fullerene fragementation process [4]. This approach shares similarities with our eccentricity-based approach, but considers only two molecules, whereas our focus is on multiple molecules (the molecule fragments).

As for the visualization of chemical processes, Wang et al. [15] present several approaches that, using machine learning techniques, build a hierarchy of the most important reactants (which correspond to the fullerene fragments in our application). Their approach shares similarities with our fragment tree approach but does not explicitly address the time-dependency of the fragmentation process. Regarding the analysis of the fragmentation distributions, they plot molecular size with respect to time, whereas we target the visualization of fragment holes due to the particular structure of fullerenes. Ahlstrom et al. [1] present a generic analysis approach that clusters trajectory snapshots, and employs techniques from network analysis. Their approach does not take into account symmetries that are inherent to fullerene fragmentation, though. More weakly related works include visualization of time-varying graphs, where nodes typically represent distinct objects. In this context, feature-based visualization, for example of communities [13] and group structures [14], is

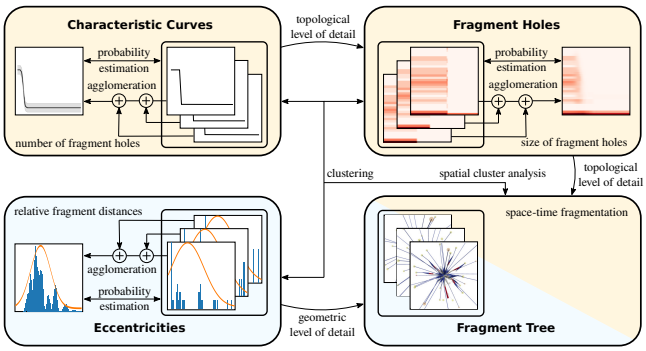

Figure 2: Overview of the interrelations and levels of detail (curved arrows pointing to finer level) between our topological (orange) and geometric (blue) components. The statistical methods agglomerate results from multiple simulations (framed image stacks) into aggregated views (single image). Their comparison serves as probability estimation of individual results. Aggregations typically contain clusters that can be inspected by spatial analysis.

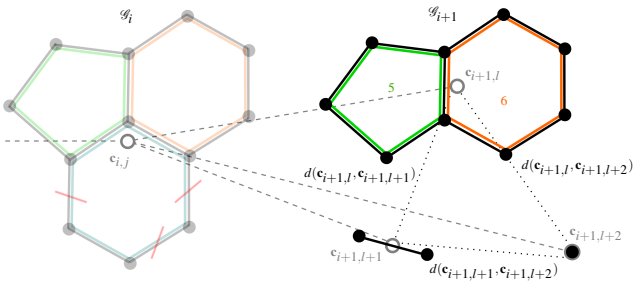

Figure 3: A fullerene fragment j (belonging to graph $\mathscr{G}_i$) with its atoms (dots) and bonds (black lines) drawn with low saturation. Three cycles are visible around its center of mass $\mathbf{c}_{i,j}$ (circle). A short time after t_i, the bonds marked in red break, resulting in one of the cycles being broken and subfragments l, $l+1$, and $l+2$ being created (each belonging to $\mathscr{G}_{i+1}$). Our method derives several quantities, namely the distances between the centers of mass (dotted lines; Section 3.1), the number of cycles (Section 3.2), cycle lengths (colored numbers; Section 3.3), and the trajectories (dashed lines) that connect fragments over space and time (Section 3.4).

particularly common. In some sense, our visualization technique is more abstract, though, and focuses on invariant properties of a graph (such as its number of cycles) because individual atoms are indistinguishable between simulations.

3 Method

Our approach is a composite technique (see Figure 2) for comparing different simulation runs of structured molecules, such as fullerenes, to reveal structural differences, and assess to what extent a simulation leads to stable results, i.e., whether sufficiently many runs of the simulation have been performed to uncover typical fragmentation behavior. Our approach is motivated by the observation that breaking molecular bonds in fullerenes, e.g., by laser pulses, causes manifold structural changes in the molecule that necessitate tailored visualization techniques. These techniques are closely integrated with the simulation, i.e., there is a tight cycle between analysis and simulation. This helps avoid costly postprocessing steps and storing all generated data.

In the following, we assume that molecules are represented as undirected graphs $\mathscr{G}_i = (V_i, E_i)$, where every atom corresponds to a vertex $v_j \in V_i$, and each bond forms an edge $(v_j, v_k) \in E_i$. We denote the initial graph of a simulation by $\mathscr{G} = (V, E)$. For a time-varying simulation with time steps $T = \{t_0, \ldots, t_m\}$, time step t_i has an associated graph $\mathscr{G}_i$. We call a connected component of $\mathscr{G}_i$ *fragment*, because it represents a fragment of the original molecule. The graphs of a simulation satisfy a nesting relationship, $\mathscr{G}_j \subseteq \mathscr{G}_i \subseteq \mathscr{G}$ for $0 \leq i \leq j \leq m$ and $V_i = V$ for all i, because the set of nodes remains the same, i.e., no atom is lost, and because, in the investigated model bonds can only break. Figure 3 illustrates a part of a fragmentation process and briefly introduces our method.

3.1 Eccentricities

Consider two separate fragmentation processes, each of which causing a molecule to lose a single atom. Suppose that, after separation, the atoms of the two processes are traveling in opposite directions. We want to consider these processes to be identical, which requires a suitable (rotation-invariant) geometrical similarity measure. Inspired by the theory of geometrical shape descriptors [17], we calculate the *eccentricity* of a set of graphs. More precisely, we represent every fragment j, i.e., every connected component, of the molecule graph $\mathscr{G}_i$ by its center of mass $\mathbf{c}_{i,j}$. We then obtain the eccentricity

$$f_e(t_i, j) := \frac{1}{k_i} \sum_{l \neq j} \mathrm{d}(\mathbf{c}_{i,j}, \mathbf{c}_{i,l}), \tag{1}$$

where $\mathrm{d}(\cdot,\cdot)$ refers to the Euclidean distance, and k_i to the number of connected components of $\mathscr{G}_i$. Calculating the eccentricity for every fragment and every time step results in a distribution (Figure 4), which we use to summarize the fragmentation process.

3.2 Characteristic Curves

The approach of Section 3.1 is geometry-based, so we complement it with a topological approach to analyze the individual graphs $\mathscr{G}_i$. Topological analysis, focusing on connectivity of the components in $\mathscr{G}_i$, has the advantage of being robust against various continuous deformations and even perturbations, while at the same time being sufficiently expressive to support data analysis. Here, we calculate the first Betti number β_1 [5, p. 130] for each $t_i \in T$, i.e.,

$$\beta_1(t_i) := m_i - n_i + k_i, \tag{2}$$

where m_i denotes the number of edges of graph $\mathscr{G}_i$, n_i the number of its vertices, and k_i its number of connected components. β_1 counts the *cycles*, i.e., structural holes, in a given graph. For example, in Figure 3, we have $\beta_1(t_i) = 14 - 12 + 1 = 3$ and $\beta_1(t_{i+1}) = 11 - 12 + 3 = 2$. When the molecule is subjected to, e.g., laser pulses, bonds are breaking down, resulting in increased fragmentation of the graph. As the number of fragments increases, however, the number of cycles necessarily needs to decrease. We obtain the *characteristic curve* of a simulation as $f_c(t) := \beta_1(t)$. Figure 5 depicts examples of characteristic curves for varying laser-excitation energies, leading to different atomic charges q (discussed in more detail below).

Since $f_c(t)$ is a piecewise linear function, calculating its mean is well-defined. This is useful because we are rarely dealing with single simulations, the stochastic nature of the experiment makes it necessary to work with ensembles of simulations. Given an ensemble that purports to model an experiment, we use the theory of bootstrap empirical processes [2] to obtain nonparametric confidence band estimates. We will use these estimates in Section 4 to determine whether a given number of simulations is suitable, or whether more simulations are required to describe the properties of the experiment.

3.3 Fragment Holes

The fragmentation of a complex molecule is a highly dynamical process with a variety of intermediate states, requiring detailed inspection of selected cases. Our characteristic curves provide the number of cycles, which is related to the number of rings in C_{60}. To study how cycles change and merge over time, we want to take their size into account. This will also help us describe the structural stability of the simulation over time.

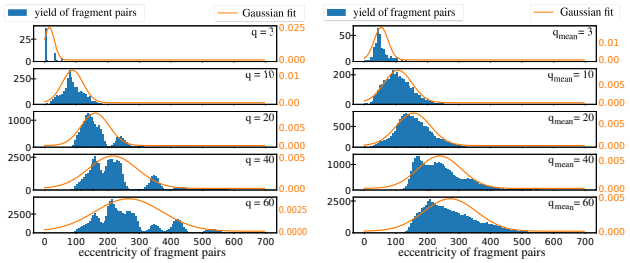

(a) Fixed charge (b) Varying charge

Figure 4: Histograms of eccentricities with Gaussian fit (orange), showing the pairwise distances of fragments at the final time step.

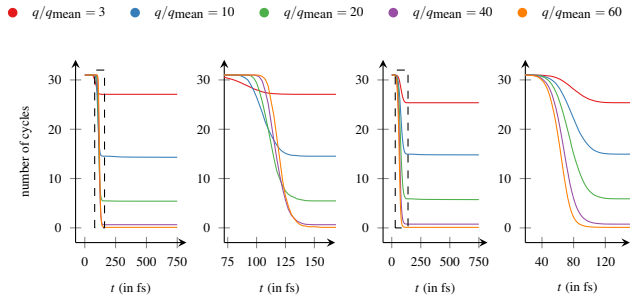

(a) Fixed charge (b) Varying charge

Figure 5: The behavior of characteristic curves for different excitation energies depends on whether a fixed charge (no stochastic variation), or a varying change (following a Gaussian distribution) is used.

As another topologically-motivated approach, we propose using the number of simple cycles, i.e., closed walks with no repetitions of edges and vertices (except for the start vertex), of the corresponding graph $\mathcal{G}_i$ at time t_i as a structural descriptor of the fragmentation process. Since enumerating all simple cycles is computationally unfeasible [7], we calculate a cycle basis [10], a minimal set of cycles that serves to describe all simple cycles of the graph. Given such a set of basis cycles $\{c_1, \ldots, c_k\}$, every cycle c of the graph can be written as $c = \sum_{i=1}^{k} \lambda_i c_i$, with $\lambda_i \in \{0,1\}$. In Figure 3, the green and orange cycle form a potential cycle basis of the highlighted connected component.

Calculating the length of every basis cycle yields a distribution of cycle lengths for every time step in the simulation. All quantities involved in these calculations are integers, so we represent a complete simulation by an $L \times |T|$ matrix M^H, where L denotes the maximum length of a cycle (i.e., the number of edges in the graph representing a molecule), and $M^H_{l,t}$ stores the number of basis cycles with length l at time step t of the simulation. Each simulation gives rise to a different M^H, so we calculate their mean and normalize over every column to ensure that we capture the most dominant cycle length per time step. We visualize the resulting matrix using a heat map. It describes the structural stability of the simulation over time—large changes in the overall structure of the matrix coincide with large changes in the topological structure of the molecule. Figure 6 depicts an example, which we will subsequently discuss in more detail.

3.4 Fragment Trees

So far, we have seen how to describe the behavior of a fragmentation process in a summarizing manner from different perspectives. However, we still need a *direct* visualization approach for individual time steps to enable a detailed understanding of selected cases. Above, we

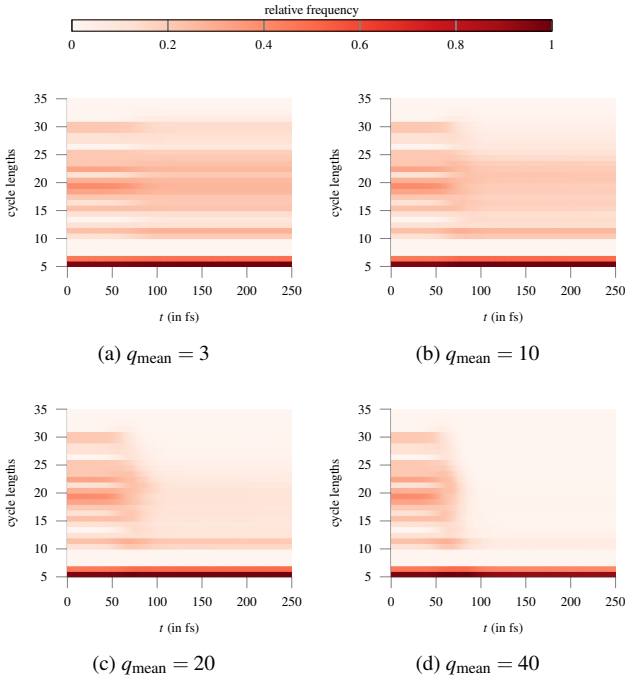

(a) $q_{\text{mean}} = 3$ (b) $q_{\text{mean}} = 10$

(c) $q_{\text{mean}} = 20$ (d) $q_{\text{mean}} = 40$

Figure 6: Simple cycles (fragment holes), averaged over simulations with varying charge q_{mean}. Only the relevant initial phase is shown.

discussed the nesting relationship of the individual graphs of a simulation. By keeping track of how the connected components change during the simulation (i.e., by keeping track of when fragments are created), we obtain the *fragment tree*. Figure 3 depicts the main idea of this representation: every directed edge of the tree represents a connected component of $\mathcal{G}_i$, and every inner node indicates a split into multiple subgraphs, providing a space–time representation of fragmentation, i.e., of fragment trajectories. To this end, we calculate the center of mass for each connected component, i.e., each fragment, and connect fragments according to the hierarchy defined by the split events.

Visual Encoding Atoms are colored by their charge to indicate repulsion due to Coulomb forces (red: strong repulsion, white: default). Bonds are colored according to the "tensions" induced by atom–atom distances. A blue–white–red color map is used to indicate distances shorter than the equilibrium distance (blueish), and larger than the equilibrium distance (reddish). Red bonds therefore indicate a potential break. The fragment tree is represented by tubes. In addition to the topological information, they encode further information via their radius and color. The tube segment of given fragment has radius proportional to its bounding sphere. The color corresponds to the maximum bond length within that fragment. In space-time representations, it can indicate separation dynamics and helps reveal temporal oscillations (striped tubes).

Variants Figure 1c depicts an example of a fragment tree. Variants of the fragment tree for the same time step are also shown in Figure 7 for comparison. Direct visualization (Figure 7a) shows the molecule fragments. Since the ball size is constant in physical space, it conveys depth. Animations could provide further temporal context, but would complicate perception. One way to provide temporal information in a stationary manner is to represent multiple time steps [3, 6] (Figure 7b), here, with a temporal resolution of 5 fs. The velocities of individual atoms are indicated by the spacing between consecutive time steps, and rotations by the "lines" of balls and "surfaces" of bonds. Nevertheless, this approach tends to suffer

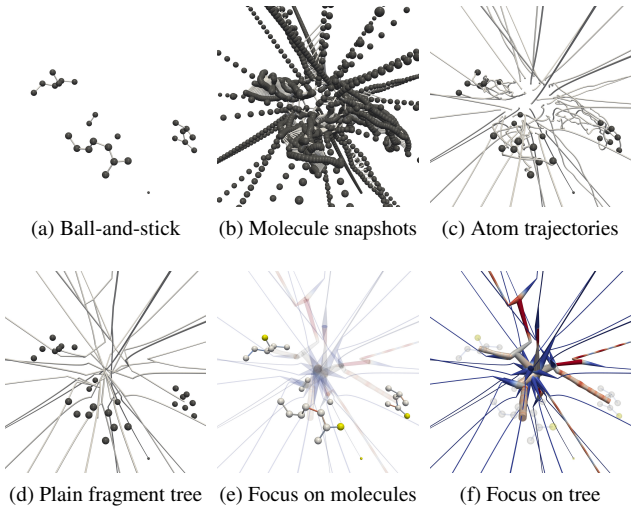

(a) Ball-and-stick (b) Molecule snapshots (c) Atom trajectories

(d) Plain fragment tree (e) Focus on molecules (f) Focus on tree

Figure 7: Comparison of spatio-temporal visualizations at example of Figure 1c. (a) Direct visualization of fragments, (b) center of mass trajectories by molecule snapshoting, (c) trajectories for each individual atom, and our fragment tree approach (d) without additional quantities, and with focus on fragments (e) and tree (f).

from visual clutter. To reduce clutter, only trajectories for each atom could be shown (Figure 7c). They are capable of visualizing paths and indicating any rotating fragments. Nevertheless, especially for larger fragments, Figure 7d demonstrates that a plain fragment tree, used in combination with direct visualization of atoms, can further reduce clutter. Clutter could also be resolved by a 2D layout of the graph. Such an approach would, however, lose geometrical information, necessitating to introduce another direct view for spatial inspection. To address possible clutter, we instead propose two transparency-based modes (Figure 7e and 7f), which focus on the fragments and the fragment tree, respectively.

4 Results

For demonstration, we overview interrelations and levels of detail between our approaches in Figure 2. From the coarsest level of detail to the finest one, we have the following steps: (i) visualization by means of eccentricities, describing the fragmentation process with respect to relative positions of the fragments, (ii) computation of characteristic curves for determining the influence of excitation energies, (iii) calculation of fragment holes for assessing the influence of different excitation energies, and (iv) interactive visualization using fragment trees to enable in-depth analysis of individual simulations. For some of these stages, we consider two models for ionization, namely *fixed charge* (i.e., assuming that the excitation of a molecule results in an instantaneous ionized charge q), and *varying charge* (where the ionization probability is proportional to a Gaussian distribution, with q_{mean} being the charge that is ionized on average). In the following, we will comment on these aspects.

Eccentricities We first consider a geometry-based analysis approach by eccentricities, analyzing the behavior of simulations for different parameters. Figure 4 depicts histograms of the eccentricity values for the last time step ($t = 750\,\text{fs}$). We first compare the behavior of fixed charges versus varying charges. For a fixed charge with $q = 3$, we obtain a peak at an eccentricity of around 3 Å. This corresponds to cases where a single atom is multiply charged, resulting in broken bonds to its neighbors, but none of these are charged, resulting in a small repelling force. For an eccentricity of 32 Å, the bonds between two neighboring atoms, each positively charged, are broken. The direct neighbors repel each other, resulting in a larger distance and thus higher eccentricity. In rare cases (eccentricity of 55 Å), two neighboring atoms lose all bonds to the rest of the fullerene. They then repel each other without bond forces. For $q_{\text{mean}} = 3$ and varying charges, we observe a larger variety of eccentricity values. This is due to the fact that more charges are possible within the molecule. Notice that the number of eccentricities is different from those of the other intensities, since it is unlikely that an atom is separated from the molecule. When we perform an overall comparison of fixed charge and varying charge, we observe that the distribution of eccentricity values appears to be normally distributed. For fixed charges, however, this is not the case.

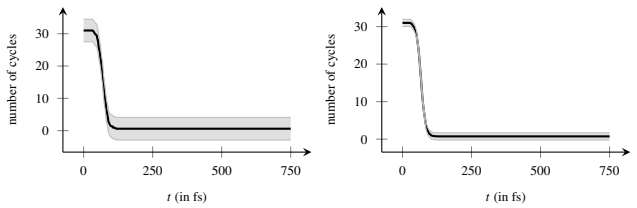

(a) 10 simulations (b) 100 simulations

Figure 8: Characteristic curves, calculated alongside the simulations, help detecting the variability of an ensemble of simulations. The 95% confidence band becomes tighter with increasing ensemble size, showing that the mean function is a suitable descriptor.

Characteristic Curves Since fragmentation experiments are highly stochastic by design, it is necessary to run numerous simulations (on the order of 10^3) in order to reasonably capture the average behavior of the system. The characteristic curves (Section 3.2) summarize the average behavior of the simulation by showing a running average of the number of cycles in the molecular graph. Since the curves are calculated alongside with the simulation, the confidence bands around the mean curve can be continuously updated as more simulations are run. Figure 8 shows the difference in confidence bands for 10 simulations and 100 simulations for $q_{\text{mean}} = 40$. For these parameters, the confidence band remains stable after approximately 100 simulations, indicating that a sufficient number of simulations have been run to study the average behavior.

We may also use this method to study the effects of parameter changes in simulations. Figure 5 shows a comparison of different excitation energies; higher excitation energies typically result in more fragments, and domain experts commonly perform simulations and experiments for different energies in order to cover a large range of conditions for real-world fragmentation processes. The simulations turn out to describe different fragmentation processes: with a fixed charge, simulations fragment almost uniformly (Figure 5a), whereas with a varying charge (Figure 5b), the difference is more distinct. Both types of simulations eventually reach the same equilibrium, though, after which no more fragments are being created. In the curves, this is indicated by a horizontal line, meaning that the number of structural holes (simple cycles) does not change anymore. We thus conclude that the difference in excitation energy is minuscule, as long as we are only interested in the end result of the fragmentation process. Understanding the differences in how fragmentation occurs, requires the fragment holes visualization, however.

Fragment Holes Analysis by means of fragment holes provides more detailed insights into the fragmentation process for varying energies. Figure 6 depicts the results for 1000 simulations each, focusing on the first 100 time steps (corresponding to 250 fs; no large changes show up afterwards). The dominant feature of every simulation, regardless of excitation energy, is a set of short cycles

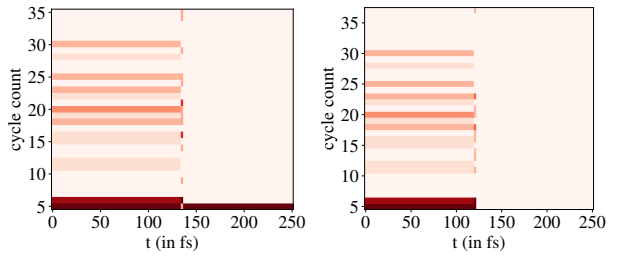

(a) Fragment holes first sample (b) Fragment holes second sample

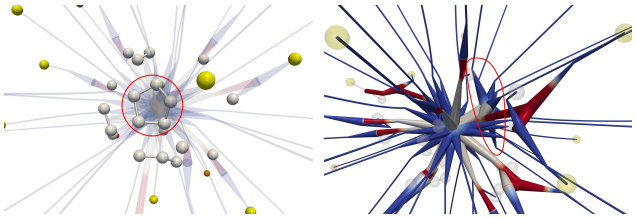

(c) Fragment tree first sample (d) Fragment tree second sample

Figure 9: (a), (b): Fragment hole visualization of two simulations with equal eccentricity values (approximately 205 Å) at the final time step. (c), (d): Corresponding fragment trees for $q = 60$ and $t = 175$ fs. Please refer to Figures 1 and 6 for the color legends.

of length 5. This means that a large part of the molecular structure remains stable over this part of the simulation. For higher excitation energies ($q_{\text{mean}} > 10$), cycles with longer lengths (> 10) rapidly vanish as the simulation progresses; already after approximately 50 time steps (125 fs), activity for higher-length cycles ceases. Notice that this is the average behavior of the fragmentation process. Individual simulations may exhibit deviations from the mean. In order to fully understand these deviations, we look at individual simulations at the most detailed level, and study the progression of the fragmentation process by means of the fragment trees.

Fragment Trees So far, all our methods provide an overview of the fragmentation process, using various different visual representations. We now want to focus on an individual simulation. The histogram of the eccentricities (Figure 4) for $q = 60$ exhibits several pronounced peaks, forming regions in the distribution. To check whether the dynamics of individual simulations within such a region are different or not, we use the fragment hole visualization approach for single time steps and observe structural differences (Figure 9a and 9b) in two selected samples. We use the fragment tree (Figure 9) to perform a detailed inspection: one of the samples has a cycle basis containing a single cycle of length 5, while the other dataset has an empty cycle basis. The remaining cycle can be easily identified in the corresponding fragment tree (Figure 9c), while the other fragment tree (Figure 9d) depicts a more complex branching in its fragmentation dynamics; we observe that one fragment even breaks into 9 subfragments, one of those branching once more (red polygon). By contrast, as shown in Figure 9c, fragmentation mainly takes place in the beginning.

5 Conclusion

In this paper, we presented a novel approach for analyzing molecule fragmentation, using the fullerene C_{60} as an example. Our approach consists of components with varying levels of detail (from coarse to fine: eccentricities, characteristic curves, fragment holes, and fragment trees). We exemplified their use to study the influence of parameters of the underlying simulations, their stability, and the fragmentation behavior of fullerenes.

There are several potential extensions for future work. First, evaluating different strategies for assessing dissimilarities of fragmentation trees (e.g., using graph Laplacians [8]) may prove useful. Second, the description of the molecular graphs and their nesting relationship enables the usage of techniques from computational topology, such as persistent homology for determining structural features [12]. One could also improve the fragment holes visualization to enumerate cycles of minimum length. This is likely to require complex heuristic search strategies, as the general problem of finding shortest cycles has an exponential complexity.

Acknowledgments

We want to thank Thomas Pfeifer and Christian Ott from the Max-Planck Institute for Nuclear Physics who helped inspire this paper. This work was supported by Forschungsallianz Baden-Württemberg, "Data-Integrated Simulation Science (DISS)".

References

[1] L. S. Ahlstrom, J. L. Baker, K. Ehrlich, Z. T. Campbell, S. Patel, I. I. Vorontsov, F. Tama, and O. Miyashita. Network visualization of conformational sampling during molecular dynamics simulation. *Journal of Molecular Graphics and Modelling*, 46:140–149, 2013.

[2] B. Efron and R. J. Tibshirani. *An Introduction to the Bootstrap*. Chapman & Hall/CRC, 1993.

[3] P. W. Fitzjohn and P. A. Bates. Guided docking: first step to locate potential binding sites. *Proteins: Structure, Function, and Bioinformatics*, 52(1):28–32, 2003.

[4] M. Gatchell. Collision induced fragmentation of molecules and molecular clusters: Knockout driven reactions in fullerenes and PAHs. Licentiate thesis, Stockholm University, 2014.

[5] A. Hatcher. *Algebraic Topology*. Cambridge University Press, 2002.

[6] W. Humphrey, A. Dalke, and K. Schulten. VMD – Visual Molecular Dynamics. *Journal of Molecular Graphics*, 14:33–38, 1996.

[7] T. Kavitha, C. Liebchen, K. Mehlhorn, D. Michail, R. Rizzi, T. Ueckerdt, and K. A. Zweig. Cycle bases in graphs: Characterization, algorithms, complexity, and applications. *Computer Science Review*, 3(4):199–243, 2009.

[8] R. Merris. Laplacian matrices of graphs: A survey. *Linear Algebra and its Applications*, 197–198:143–176, 1994.

[9] B. Murphy, T. Osipov, Z. Jurek, L. Fang, S. Son, M. Mucke, J. Eland, V. Zhaunerchyk, R. Feifel, L. Avaldi, P. Bolognesi, C. Bostedt, J. Bozek, J. Grilj, M. Guehr, L. Frasinski, J. Glownia, D. Ha, K. Hoffmann, E. Kukk, B. McFarland, C. Miron, E. Sistrunk, R. Squibb, K. Ueda, R. Santra, and N. Berrah. Femtosecond X-ray-induced explosion of C_{60} at extreme intensity. *Nature Communications*, 5(4281), June 2014.

[10] K. Paton. An algorithm for finding a fundamental set of cycles of a graph. *Communications of the ACM*, 12(9):514–518, Sept. 1969.

[11] S. Plimpton. Fast parallel algorithms for short-range molecular dynamics. *Journal of Computational Physics*, 117(1):1–19, 1995.

[12] B. Rieck, U. Fugacci, J. Lukasczyk, and H. Leitte. Clique community persistence: A topological visual analysis approach for complex networks. *IEEE TVCG*, 24(1):822–831, 2017.

[13] C. Vehlow, F. Beck, P. Auwärter, and D. Weiskopf. Visualizing the evolution of communities in dynamic graphs. *Computer Graphics Forum*, 34(1):277–288, 2015.

[14] C. Vehlow, F. Beck, and D. Weiskopf. Visualizing group structures in graphs: A survey. *Computer Graphics Forum*, 36(6):201–225, 2017.

[15] L.-P. Wang, A. Titov, R. McGibbon, F. Liu, V. S. Pande, and T. J. Martínez. Discovering chemistry with an ab initio nanoreactor. *Nature Chemistry*, 6(12):1044–1048, 2014.

[16] K. Yamazaki, T. Nakamura, N. Niitsu, M. Kanno, K. Ueda, and H. Kono. Two-step explosion processes of highly charged fullerene cations C_{60}^{q+} (q = 20–60). *The Journal of Chemical Physics*, 141(12):121105:1–4, 2014.

[17] D. Zhang and G. Lu. Review of shape representation and description techniques. *Pattern Recognition*, 37(1):1–19, 2004.